

Density functional and classical simulations of liquid and glassy selenium

J. Kalikka¹, J. Akola^{1,2}, R. O. Jones^{3,*} and H. R. Schober⁴

¹Computational Physics Laboratory, Tampere University, FI-33014 Tampere, Finland

²Department of Physics, NTNU Norwegian University of Science and Technology, NO-7491 Trondheim, Norway

³Peter-Grünberg-Institut (PGI-1) and JARA/HPC, Forschungszentrum Jülich, D-52425 Jülich, Germany

⁴Peter-Grünberg-Institut (PGI-2) and JARA/HPC, Forschungszentrum Jülich, D-52425 Jülich, Germany



(Received 29 June 2020; accepted 28 August 2020; published 22 September 2020)

Molecular dynamics simulations of liquid and glassy selenium have been carried out using density functional (400–773 K, 600 atoms) and classical force field (290–500 K, 5488 atoms) methods. Structural features (structure factors, pair distribution functions, bond lengths, bond and dihedral angles, cavities) and dynamical properties (diffusion coefficients, power spectra, sound velocity, collective excitations, bond lifetimes) agree well with experimental data where available. The structures are predominantly chainlike, with a small fraction of rings with a range of sizes, and large cavity volumes lead to flexible chains. It is striking that the density functional simulations show very few Se₈ rings at 600 K and below.

DOI: [10.1103/PhysRevB.102.104202](https://doi.org/10.1103/PhysRevB.102.104202)

I. INTRODUCTION

The properties of chalcogen elements (group 16, valence configuration ns^2np^4), particularly S, Se, and Te, have fascinated researchers for more than a century. Chalcogen atoms have two “lone pair” p electrons occupying nonbonding, directional orbitals at the top of the valence band, and a well-known preference for divalency and twofold coordination [1]. Many structures contain rings and chains, where the bond angles α are dominated by the overlap of the p orbitals, and the dihedral angles γ reflect the repulsion of $p\pi$ electrons on “lone pair” orbitals, which is weakest when the orbital planes are orthogonal. Simple considerations favor narrow ranges for α (95° – 110°) and γ (70° – 100°) [2], and helical forms of these elements should have low torsion barriers (~ 0.1 eV) [3].

Sulfur has the most solid allotropes (>30) of any element [4] including helices and unbranched cyclic molecules S_n ($n = 6$ – 20). Rings, chains, and helices also occur in Se and Te, and the structures (S [5–7], Se [8,9], Se_{*x*}S_{*y*} [10], Te [11]) show clear trends as the atomic number Z increases: The coordinates of the ring structures scale systematically, and the ratio between the interchain and intrachain distances in fibrous S and the α forms of Se, Te, and Po decreases steadily. Trends in the electronic properties of the crystals are the same as in groups 14 and 15: insulator (S) to semiconductor (Se, Te) to metal (Po).

In spite of these structural regularities and the miscibility for all concentrations of S-Se, S-Te (with a gap [12,13]), and Se-Te [14,15], the *disordered* phases of S, Se, and Te differ greatly, as emphasized in a recent review [16]. It has been known for over a century [17] that the viscosity of liquid S increases by several orders of magnitude near 160 °C. This is usually attributed to the ring-opening polymerization of S₈ units [18], and very recent combined density, x-ray diffraction, and Raman scattering measurements in sulfur indicate

the presence of a liquid-liquid first-order phase transition and critical point at pressures up to 3 GPa [19]. Eisenberg and Tobolsky [20] proposed that a ring-chain transition also occurred in Se at 356 K, i.e., *below* the melting point (494 K). Misawa and Suzuki [21] developed a disordered chain model incorporating chains and Se₈ conformations in a single molecule, and Böhmer and Angell [22] viewed changes of tensile modulus and stress relaxation as evidence for a transition involving rings and chains near 300 K, slightly below the glass temperature. The difference between the dominant Raman-active modes in trigonal Se (A_1 , 233 cm^{-1}) and in amorphous and monoclinic Se (250 cm^{-1}) has been interpreted as the signature of Se₈ rings in the glass [23]. However, Se₅, Se₆, and Se₇ molecules are more prevalent than Se₈ in the vapor above liquid Se [24], indicating their presence in the liquid. The crystal structures of Se₆, Se₇, and Se₈ are known [4].

An alternative picture is provided by viscosity and recoverable creep compliance measurements [25], which indicate that amorphous Se is a relatively low molecular weight polymer *without* rings. Warren and Dupree [26] attributed shifts in ⁷⁷Se nuclear magnetic resonance (NMR) data to paramagnetic centers at the chain ends and concluded that the chains comprised about 750 atoms at 873 K and many more at temperatures near the melting point. A reverse Monte Carlo (RMC) study of neutron diffraction data indicated that the prevalence of chainlike molecules was “more probable” than rings in amorphous Se [27]. Furthermore, ⁷⁷Se NMR spectroscopy can distinguish readily between chains in trigonal crystalline Se and cyclo-Se₈ rings in the monoclinic forms provided no evidence for such rings in amorphous Se [28]. Rheological measurements on supercooled Se showed the presence of two distinct relaxation processes coupled to viscosity, but with timescales differing by several orders of magnitude [29].

Liquid Se is a polymeric semiconductor at normal temperatures and pressures, but it is metallic above 1700 K and 38.5 MPa [30]. The semiconductor-metal transition has been attributed to a structural change from helical to planar zigzag chains [31] accompanied by changes in the distribution

*r.jones@fz-juelich.de

of voids [32]. Density functional calculations show indeed that the conduction and valence bands of the planar zigzag structure overlap [9]. For temperatures between 343 K (superheated glass) and 441 K (supercooled liquid), spontaneous crystallization means that a disordered, metastable state is unsustainable over long periods [33]. There are no viscosity data in this temperature range, but shorter measurements may produce useful data for other quantities.

Rings and chains have the lowest energy of small aggregates of Te atoms [11], but there are no molecular allotropes of the element and no evidence for Te_8 rings in liquid Te. The properties of *disordered* Te are also unusual: The liquid can be supercooled to 553 K [34], far below the melting point (722 K), near which a maximum in the density and a semiconductor-metal transition occur [34]. At 626 ± 3 K there are extrema in the specific heat, thermal expansion coefficient, compressibility, and related properties that point to a structural phase transition. Amorphous thin films of Te on a cold substrate crystallize when warmed above 285 K.

There have been many molecular dynamics (MD) simulations of disordered phases of S, Se, and Te using classical force fields (FF) and density functional (DF) [35] calculations. The former can be carried out for thousands of atoms and hundreds of nanoseconds and include simulations of amorphous and liquid Se [36–39], and there have been Monte Carlo studies of the equilibrium polymerization of liquid S [40] and liquid Se [41]. The last of these used a semiempirical tight-binding model, and others [36,38,40,42] used FF fitted to measured quantities and the results of DF calculations on small atomic aggregates. DF calculations are often free of adjustable parameters, but they are computationally very demanding for large systems, and early DF calculations on disordered Se [43–45] and liquid Te [46] were restricted to small samples (<100 atoms) and short times ($\lesssim 10$ ps). Much longer DF calculations on larger samples of liquid [47] and amorphous [11] Te led to more convincing results.

Se is the only element with a glass transition temperature near 300 K, where the viscosity is 12 orders of magnitude higher than at the melting point [48]. MD simulations are very challenging in the liquid and glassy states, and long simulation times are essential. We study here structural patterns, pair distribution functions $g(r)$ and structure factors $S(q)$, and dynamical properties (diffusion coefficients, power spectra, bond lifetimes) using dynamical structure factors $S(q, \omega)$ and current-current correlation functions. We compare with experimental results, particularly quasielastic and inelastic neutron scattering [49–51] and inelastic x-ray scattering (IXS) [52], which provide information about collective excitations. The DF/MD method was used previously to study liquid Te [47], Bi [53], and Sb [54], and details are given in [53]. In Sec. II we summarize the methods of calculation and the basis of the analysis, and the results are presented and discussed in Secs. III and IV, respectively.

II. METHODS OF CALCULATION

A. Classical molecular dynamics

Classical MD (FF) simulations with periodic boundary conditions were performed on 10 independent systems of 5488 atoms [39] interacting with a three-body potential [42]

with parameters adjusted to reproduce properties of Se clusters and the trigonal crystalline phase. This force field has proved to be useful in a range of contexts [37,55,56]. The pressure was set to zero throughout the constant pressure (NPT) simulations by using a Parrinello-Rahman algorithm [57] with mass parameter $W = \sqrt{N} m_{\text{Se}}$, where N is the number of atoms in the sample and m_{Se} the mass of the Se atom. A small volume damping term was added to reduce volume fluctuations at high temperatures. The equations of motion were integrated using the velocity Verlet algorithm [58] with a time step of 1 fs. The 10 samples were initially equilibrated at 650 K, quenched at a rate of 10^{12} K/s, and aged at a constant temperature for up to 800 ns. Some expanded simulations with 148 176 atoms were carried out at 350 K and 500 K. More details are given in [39].

B. Density functional calculations

The DF/MD simulations (DF) were carried out with the CPMD program [59] in the Born-Oppenheimer MD mode. Periodic boundary conditions and a single point ($k = 0$) in the Brillouin zone were used, and the electron-ion interaction was represented by a scalar-relativistic Trouiller-Martins pseudopotential [60] for the valence electrons of Se ($4s^2 4p^4$). We used the PBEsol approximation [61] for the exchange-correlation energy functional and a plane wave basis with a kinetic energy cutoff of 25 Ry.

The simulations were performed with 600 Se atoms in cubic simulation boxes (27.01667 \AA) of fixed volume (NVT ensemble) with a time step of 3.0236 fs. The experimental density at the melting point (3.99 g cm^{-3} , number density $0.03043 \text{ atoms \AA}^{-3}$) [62,63] was used throughout, although somewhat lower densities may have been preferable at higher temperatures (e.g., 3.56 g cm^{-3} at 773 K [62]). The temperature was controlled by a Nosé-Hoover thermostat [64], and samples were equilibrated at each temperature before data collection, which took 75 ps at 600 K, 773 K; 140 ps at lower temperatures. The pressures (average of the stress tensor diagonal components) were 13.9 kbar at 773 K and 12.7 kbar at 500 K, which are typical values for DF simulations of this scale.

1. Structure factor, pair distribution function

If \vec{r}_i denotes the coordinates of atom i and \vec{r}_{ij} the vector between atoms i and j , the pair distribution function (PDF) $g(r)$ is the spherical average over configurations

$$g(r) = \frac{1}{\rho} \left\langle \sum_i \sum_{j \neq i} \delta(r - |\vec{r}_{ij}|) \right\rangle, \quad (1)$$

where ρ is the atomic number density. The local structure is also characterized by the distributions of bond angles, near-neighbor separations, and ring structures. Cavities (nanosized empty regions) were assigned by using a cubic mesh and determining domains (grid points) that are farther from any atom than a given cutoff (here 2.6 \AA) and constructing cells around them according to the Voronoi prescription [65].

The structure factor $S(q)$ is the Fourier transform of $g(r)$:

$$S(q) = 1 + \rho \int_0^\infty dr 4\pi r^2 [g(r) - 1] \frac{\sin(qr)}{qr}. \quad (2)$$

The coordinates and velocities of all atoms are monitored throughout, so that distributions of bond lengths and bond and dihedral angles can be determined. The definition of the dihedral angle follows Klyne and Prelog [66].

2. Power spectrum and thermodynamics

The particle velocities \vec{v}_i lead to the velocity-velocity autocorrelation function C_v ,

$$C_v(t) = \frac{1}{N} \sum_{i=1}^N \frac{\langle \vec{v}_i(0) \cdot \vec{v}_i(t) \rangle}{\langle \vec{v}_i(0) \cdot \vec{v}_i(0) \rangle}, \quad (3)$$

whose Fourier transform is the vibrational density of states (vDOS) or power spectrum. The power spectrum can be decomposed into ‘‘gas phase’’ (g, diffusive, single-particle) and ‘‘solid’’ (s, collective) components, which contribute to the low- and high-frequency regimes, respectively. This is the basis of the TwoPT (two phase thermodynamics) program [67] used here, where the diffusional component is modeled by a hard sphere gas. The *fluidicity* f is the fraction of the degrees of freedom of the system that are diffusional.

The diffusion coefficient D can be determined from the mean-squared displacements (MSD) of the atoms (coordinates \vec{r}_i), and we write its long-time limit as

$$D_\infty = \lim_{t \rightarrow \infty} \frac{\langle |\vec{r}_i(t) - \vec{r}_i(0)|^2 \rangle}{6t}. \quad (4)$$

It is convenient to introduce a time-dependent diffusion coefficient

$$D(t) = \frac{1}{6} \frac{d}{dt} \langle s^2(t) - s_{\text{ball}}^2 \rangle, \quad (5)$$

where s denotes the atomic displacement and s_{ball} accounts for displacements due to ballistic motion and/or vibrations. Changes in D in a model glass beyond a waiting time t_w can be fitted well using parameters of a ‘‘defect’’ model [68]

$$D(T, t) = D_\infty(T) + D_{\text{def}}(T) c_{\text{def}}(T, t_w) e^{-\alpha_D(T)(t-t_w)}, \quad (6)$$

and we use this form in Sec. III B 1.

3. Dynamical structure factor

The density fluctuations in the liquid can be described by the intermediate scattering function

$$F(\vec{q}, t) = \langle \text{Re}[n(\vec{q}, t + t_0)n(\vec{q}, t_0)] \rangle, \quad (7)$$

where $\langle \dots \rangle$ denotes an average over all reference times t_0 , and $n(\vec{q}, t)$ is a Fourier component of the density,

$$n(\vec{q}, t) = \frac{1}{\sqrt{N}} \sum_i \exp(i\vec{q} \cdot \vec{r}_i). \quad (8)$$

The index i runs over all N particles.

The dynamical structure factor $S(\vec{q}, \omega)$ is the Fourier transform of $F(\vec{q}, t)$,

$$S(\vec{q}, \omega) = \frac{1}{2\pi} \int dt F(\vec{q}, t) \exp(i\omega t). \quad (9)$$

The wave number \vec{q} is restricted by the periodic boundary conditions to

$$q = |\vec{q}| = \frac{2\pi}{L} |(n_1, n_2, n_3)|, \quad (10)$$

where n_1, n_2 , and n_3 are integers and L is the size of the cubic simulation cell. $F(\vec{q}, t)$ can also be obtained directly from the (van Hove) time-dependent pair distribution function $g(r, t)$, but the Fourier transform of the current densities yielded more stable results.

4. Current autocorrelation functions

The current autocorrelation function $C(\vec{q}, t)$ [69] can be calculated from the Fourier transform of the particle current $J(\vec{q}, t)$, which has a longitudinal component

$$J_L(\vec{q}, t) = \frac{1}{\sqrt{N}} \sum_i \vec{q} \cdot \vec{v}_i \exp(i\vec{q} \cdot \vec{r}_i) \quad (11)$$

and a transverse component

$$J_T(\vec{q}, t) = \frac{1}{\sqrt{N}} \sum_i \vec{q} \times \vec{v}_i \exp(i\vec{q} \cdot \vec{r}_i). \quad (12)$$

The current autocorrelation function also has longitudinal

$$C_L(\vec{q}, t) = \langle \text{Re}[J_L(\vec{q}, t + t_0)J_L(\vec{q}, t_0)] \rangle \quad (13)$$

and transverse components

$$C_T(\vec{q}, t) = \frac{1}{2} \langle \text{Re}[J_T(\vec{q}, t + t_0)J_T(\vec{q}, t_0)] \rangle. \quad (14)$$

More details are provided in [70].

5. Viscosity

The shear viscosity η arises from coupling to transverse modes and may be determined, in principle, from $C_T(\vec{q}, t)$. In liquid bismuth, the viscosity changes by only a factor of two between 573 K and 1023 K, and such an analysis led to very good agreement with experiment [70]. A simple connection between viscosity η and diffusion coefficient D is the Stokes-Einstein relationship (SER) [71], which was derived for the diffusion of uncorrelated macroscopic spheres in a liquid:

$$D(T)\eta(T) = \frac{k_B T}{c\pi d}, \quad (15)$$

where d is the effective diameter of a sphere, and c depends on the boundary conditions between the particle and fluid (slip: $c = 2$; stick: $c = 3$). The SER is often satisfied (within $\sim 20\%$) for monatomic liquids and simple molecules at high temperatures, and liquid Bi is a good example [70].

The situation in Se is dramatically different. The viscosity at the glass transition temperature (~ 300 K) is at least 13 orders of magnitude higher than in the liquid at 600 K [48], and the values depend on the method of measurement used. Furthermore, early neutron scattering measurements on Se at 523 K and above led to an activation energy for diffusion of 5.0 kcal/mole [49], which is much less than the apparent activation energy for viscous flow (18 kcal/mol [72]). Two dynamical processes are crucial in liquids of group 16 elements: diffusional motion of chain segments and bond interchange [73,74]; the highly correlated atomic motions in Se chains mean that large violations of the SER can be expected ([49], Fig. 5). Extensive analysis of the present simulations showed that the connection between $C_T(\vec{q}, t)$ and η , used successfully in liquid Bi, is inappropriate for disordered Se and was not pursued.

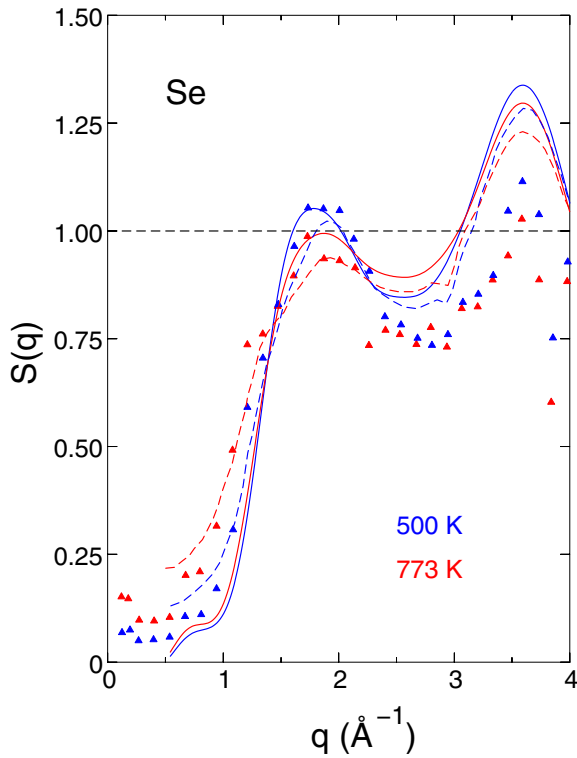


FIG. 1. Structure factors $S(q)$ calculated (DF) for 500 K (full blue curve) and 773 K (full red curve) compared with IXS measurements [52] at 523 K (blue triangles) and 773 K (red triangles) and IND measurements [51] at 503 K (dashed blue curve) and 773 K (dashed red curve) (after [52]).

III. RESULTS

After presenting details of the structures, we focus on the dynamical (time-dependent) aspects. Our main emphasis is on the DF results, and the FF simulations provide additional insight. Coordinate files for the final DF structures at 500 K, 600 K, and 773 K are provided as Supplemental Material [75] and can be visualized using freely available software [76].

A. Structural properties

1. Pair distribution function $g(r)$, structure factor $S(q)$

In Fig. 1 we compare the calculated structure factors at 500 K and 773 K with the experimental (IXS) values of Inui *et al.* at 523 K and 773 K [52] and inelastic ND results [51], as given in [52]. The pair distribution functions $g(r)$ for the DF calculations at 400, 450, 500, 600, and 773 K are shown in Fig. SF1 in the Supplemental Material [75], and the corresponding structure factors for q up to 12 \AA^{-1} are shown in Fig. SF2.

The coordination number, usually defined by the integral over $g(r)$ to the first pronounced minimum, is close to 2.0 in all studies of amorphous Se, and the present studies are no exceptions. This is consistent with both ring and chain structures and in broad agreement with the picture of Pauling [2], where bond lengths and the bond and dihedral angles vary within relatively narrow ranges.

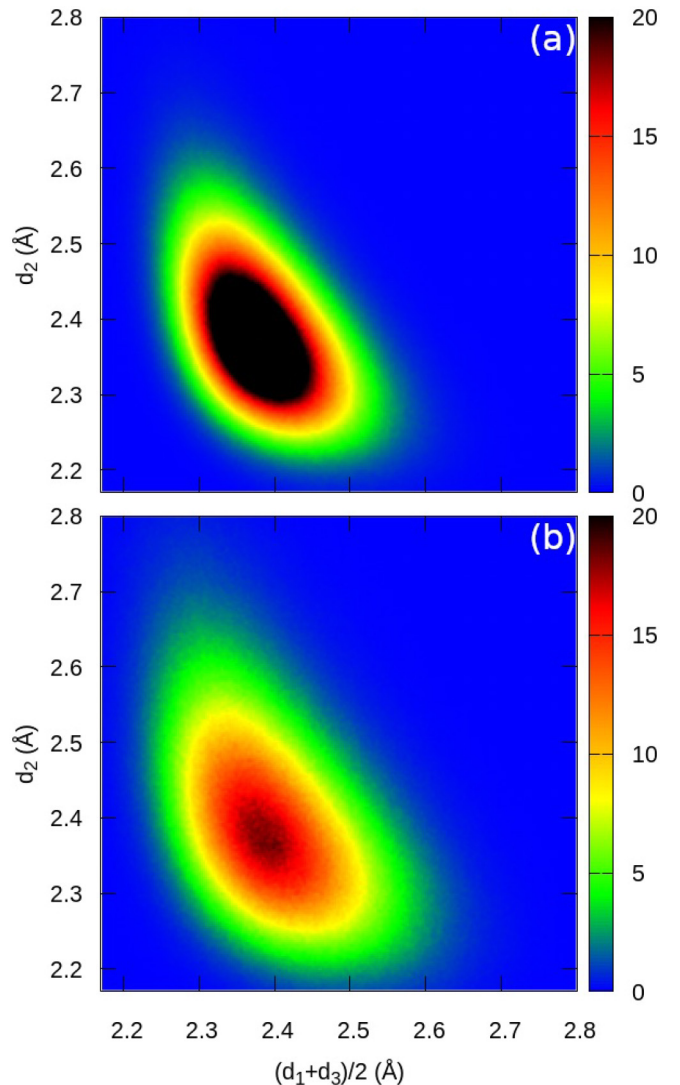


FIG. 2. Color maps of bond lengths (d_2) of twofold-coordinated atoms against the average of bonds to neighboring atoms (d_1 , d_3) for (a) 500 K and (b) 773 K. The origins of the axes correspond to the interatomic separation in Se_2 (2.17 Å).

2. Chains, coordination defects

For temperatures of 600 K and below, there are chains of more than 500 atoms (of the 600 in the DF simulation cell) that stretch across cell boundaries. The large fraction of atoms belonging to a “chain” makes it difficult to differentiate them from “rings” (see below), and the effect of periodic boundary conditions is greater than in the much larger FF simulations. If chain ends are identified in the FF results by atoms with a coordination number other than 2, we find about 80% of the atoms are in chains, and the average chain at 350 K has around 50 atoms.

Steudel and coworkers [77] found that the longest bonds in sulfur ring molecules are always adjacent to short bonds. In fact, the bond length (d_2) is approximately inversely related to the mean of the two neighboring bonds (d_1 , d_3). An analysis of calculated bond lengths in S_n molecules ($n = 2-13$) [43] found the same inverse relationship. Color maps of these two quantities are shown in Fig. 2 for all four-atom chain segments

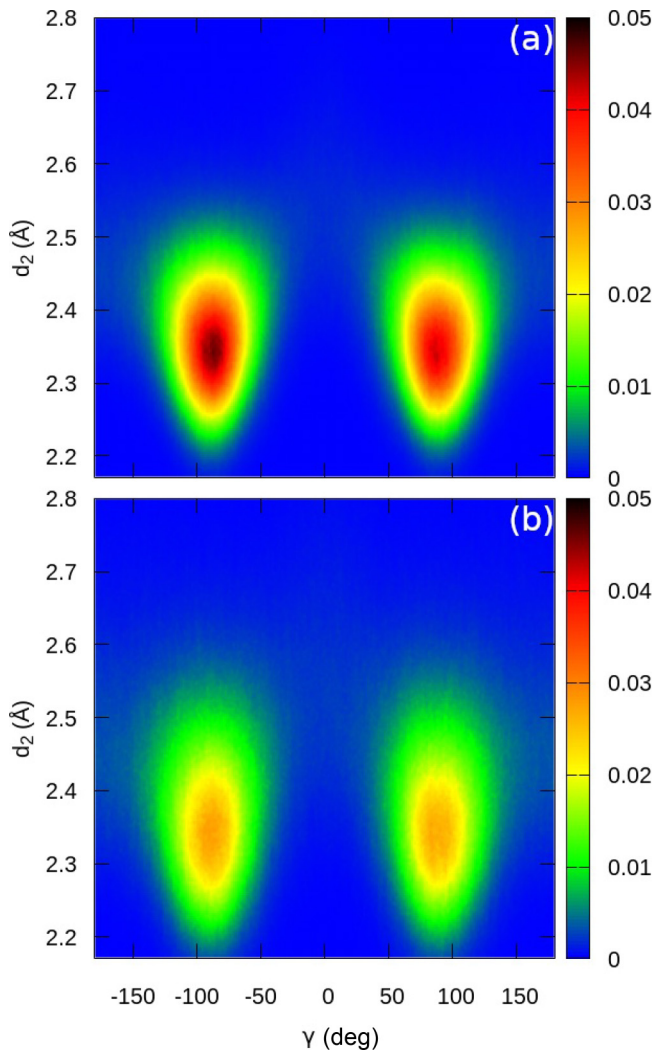


FIG. 3. Color maps of bond lengths d_2 of twofold-coordinated atoms against the dihedral angle γ for 500 K (upper) and 773 K (lower). The origin of the d_2 axis corresponds to the interatomic separation in Se_2 (2.17 Å).

occurring in the simulations at 500 K and 773 K, where the central pair are each twofold coordinated. The trend found in sulfur rings is then repeated in disordered Se, and similar plots are found at lower temperatures. The larger atomic motions found at 773 K are reflected in the fuzzier plot for this temperature.

The second empirical relation that was supported by calculations on S_n molecules is that d_2 is shortest for dihedral angles γ near 90° . For the same sequences of four atoms, we show the relationship between these quantities in Fig. 3. Dihedral angles near $\pm 90^\circ$ are preferred, and there are very few structures with γ near 0° , which occur in Se_n molecules, or 180° , as found in the planar zigzag structure of the Se_∞ helix. This structure has an energy only 0.2 eV/atom above the trigonal form [9], and structures with positive and negative dihedral angles are almost equally likely.

Structures with higher coordination numbers are uncommon, but significant, and early DF/MD simulations indicated that single threefold coordinated atoms were the most common defect [43]. Nevertheless, the small (64-atom) simulation cell and the relatively short timescales certainly overestimated the number of defects. Extended x-ray absorption fine structure (EXAFS) measurements [78] showed that the coordination number increased by 20% (to 2.2) after irradiation, which was attributed to the transient formation of static threefold-coordination sites. The dominant coordination defects in the present DF simulations also have threefold coordination, i.e., three atoms within 2.8 Å, and 0.29% and 2.02% of the atoms are threefold coordinated at 500 K and 773 K, respectively. Only 0.01% of the atoms are fourfold coordinated at 773 K. These fractions are much lower than those found in an RMC analysis of neutron diffraction measurements on liquid Se at 523 K and 623 K, where around 30% of the atoms were threefold and around 5% fourfold coordinated [79].

If “short” bonds are those shorter than 2.6 Å, threefold-coordinated defects with one long and two short bonds dominate at all temperatures, although the dominance becomes weaker as the temperature increases. At 773 K, 67% of the threefold sites have one long and two short bonds, but 25% have two long bonds, and 7% have three short bonds. The last of these are the most prevalent in the classical FF simulations. Bond angle distributions (for twofold- and threefold-coordinated atoms) are shown for temperatures 500 K and 773 K in Fig. 4. Apart from the prominent peaks $\sim 100^\circ$ – 110° , the distributions show few features, but the range of sizes is greater at 773 K. The early DF results [43] are similar and also show enhanced weight for threefold-coordinated structures with $\alpha \sim 160^\circ$.

3. Rings

Chains are the dominant structural feature, but there have been many studies of rings in disordered chalcogens, particularly those with eight atoms. Ring distributions here are found by searching for all unique closed loops of bonded atoms. A loop shaped like a figure 8, for example, would contain one large and two smaller rings. The closed chainlike features mentioned above are included and are present throughout the simulations at 500 K and below, and for part of the simulation at 600 K. They do not occur at 773 K, where there is a broader range of smaller ring sizes. The distributions of rings containing 30 and fewer atoms are shown for 500 K and 773 K in Fig. 5 for a bond cutoff of 2.8 Å. Shorter cutoffs reduce the number of rings, but the overall picture is unchanged. The most striking result for smaller ring sizes is the absence of Se_9 rings at 500 K and below.

The FF simulations at 350 K and 500 K are much longer than the DF simulations, and the much larger samples make the effect of periodic boundary conditions weaker. In addition to very long chains with ends defined by singly coordinated atoms, there was a range of smaller Se_n rings with $5 \leq n \lesssim 15$, with Se_5 dominant. Eight-membered rings occurred, and the number of smaller rings of different sizes varied more than in MD/DF simulations (Fig. 5). Increasing the pressure in

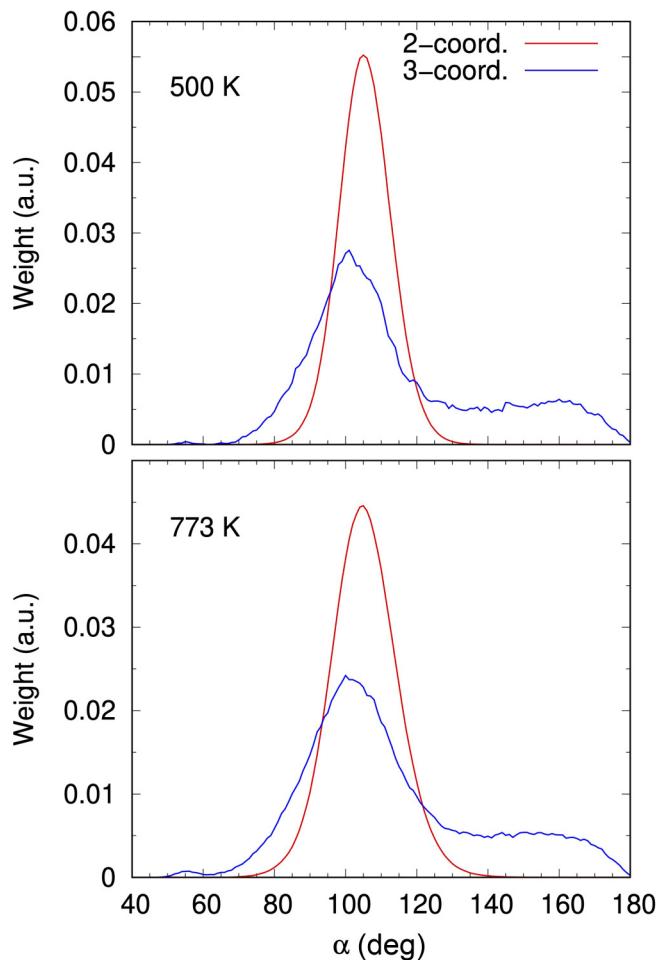


FIG. 4. Distribution of bond angles α for twofold- and threefold-coordinated atoms at 500 K (above) and 773 K (below).

the simulation to 5 GPa produced little change in the ring distributions.

4. Cavities

The surface-based cavities [65] for a representative structure of Se at 500 K (just above the melting point) are shown in Fig. 6. The cutoff distance r_c of 2.6 Å allows a direct comparison with the results for amorphous Te [11], where the larger cutoff (2.8 Å) reflects the larger atomic radius and longer bonds. The cavity volume is approximately constant (48%–50%) in the temperature range 400–773 K, and the optimized structure of amorphous Te had a substantially lower cavity volume (37%) [11].

The origin of the first sharp diffraction peak or prepeak in $S(q)$ has been discussed on numerous occasions in the context of medium-range order and related to the clustering and ordering of structural units, including voids [80,81]. Caprion and Schober [37] performed FF simulations on liquid and amorphous Se and found at lower density a prepeak at $\sim 1.3 \text{ \AA}^{-1}$ that was absent at higher density, and they attributed this to correlations between voids. Ordering of voids and Se chains has also been used to explain EXAFS and neutron diffraction measurements on liquid Se and Rb-Se mixtures [51]. The void concentration increased with increasing temperature.

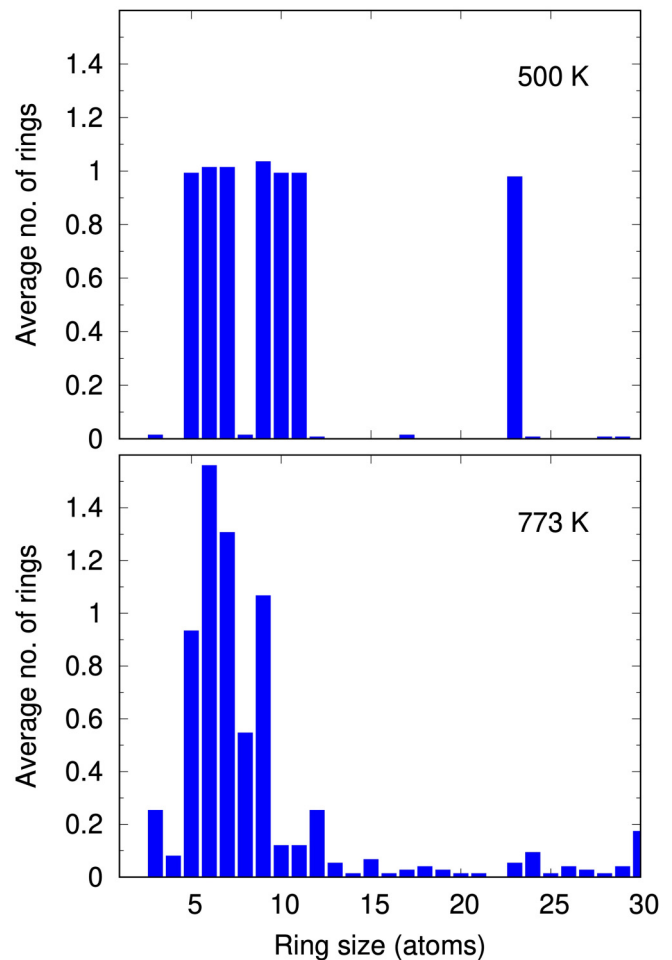


FIG. 5. Average number of rings with less than 30 atoms during 600-atom simulations at 500 K and 773 K. The bond cutoff is 2.8 Å.

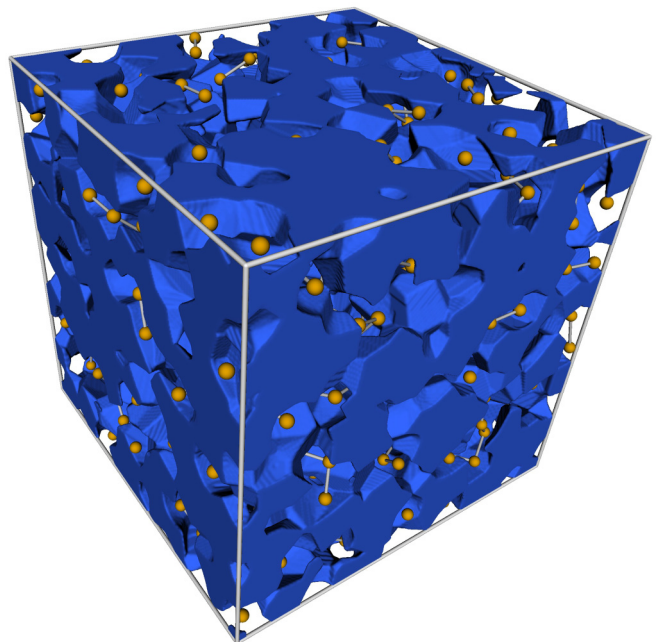


FIG. 6. Surface-based cavities (blue) in unit cell of Se (brown atoms) at 500 K using cutoff radius of 2.6 Å.

TABLE I. Diffusion coefficient D_∞ [Eq. (6); FF simulations], D (DF simulations) from mean-squared displacements and TwoPT program, and fluidicity f (TwoPT program) at five temperatures. The units of D are 10^{-5} cm²/s.

T (K)	D_∞ (FF)	D (DF) MSD, TwoPT	f
400	0.108	0.027, 0.048	0.038
450	0.329	0.052, 0.082	0.049
500	0.677	0.096, 0.178	0.059
600		0.216, 0.293	0.092
773		0.581, 0.786	0.146

A prepeak in $S(q)$ near 1 \AA^{-1} is not resolved in the IXS and IND measurements (Fig. 1), and definite identification in the DF results is not possible (Fig. 1). The presence of multicavities corresponding to more than one domain complicates the analysis. Nevertheless, ordering in the cavities can be studied by calculating the partial pair distribution functions involving the centers of domains or cavities (cav) and Se atoms, $g(r)_{\text{Se-cav}}$ and $g(r)_{\text{cav-cav}}$ (Fig. SF7). The former shows weak peaks near 4.9 \AA and 6.4 \AA , and the latter a maximum at $r = 5.2 \text{ \AA}$. The noisy data do not allow Fourier transformations, but the peak in $g(r)_{\text{cav-cav}}$ suggests a q value in the range $1.0\text{--}1.2 \text{ \AA}^{-1}$, where the prepeak indeed occurs. These and other published cav-cav PDFs are noisy and depend on the definition of “cavity” or “void” adopted, and the results should be treated with caution.

B. Dynamical properties

1. Diffusion coefficient

The diffusion coefficients D_∞ (FF) and D (DF) are given in Table I at several temperatures. Values of D were calculated from mean-squared displacements and from the TwoPT program [67] (Sec. II B 2), which also provides values of the fluidicity (Table I). The values of D are in reasonable agreement, which suggests that the approximation of the diffusional modes by those of a hard sphere gas is satisfactory in this chainlike system. We know of no direct measurements of D in amorphous Se, e.g., by using radioactive ^{75}Se as tracer. Indirect methods, such as measuring the broadening of the quasielastic peak in neutron scattering, lead to inconsistent results [49,82]. The values of D in Table I are in reasonable agreement with those in [49] ($\sim 0.4 \times 10^{-5}$ cm²/s at 523 K) and of DF/MD simulations on small samples ($< 0.5 \times 10^{-5}$ cm²/s at 570 K [45]), but are much larger than those of [82] (2.2×10^{-7} cm²/s at 500 K).

TwoPT calculations require relatively short trajectories, but equilibration is difficult to achieve below 500 K on times accessible to the present DF simulations. Figure 7 shows D_∞ and the corresponding decay constants α [Eq. (6)] after an FF simulation of 5 ns for temperatures between 500 K and 290 K, and it is clear that long simulations are essential at low temperatures. The MD/DF simulation times of 140 ps at 450 K and below are unlikely to have reached equilibrium, and we focus here on the DF simulations at 500 K and 773 K, where experimental results are available, and 600 K.

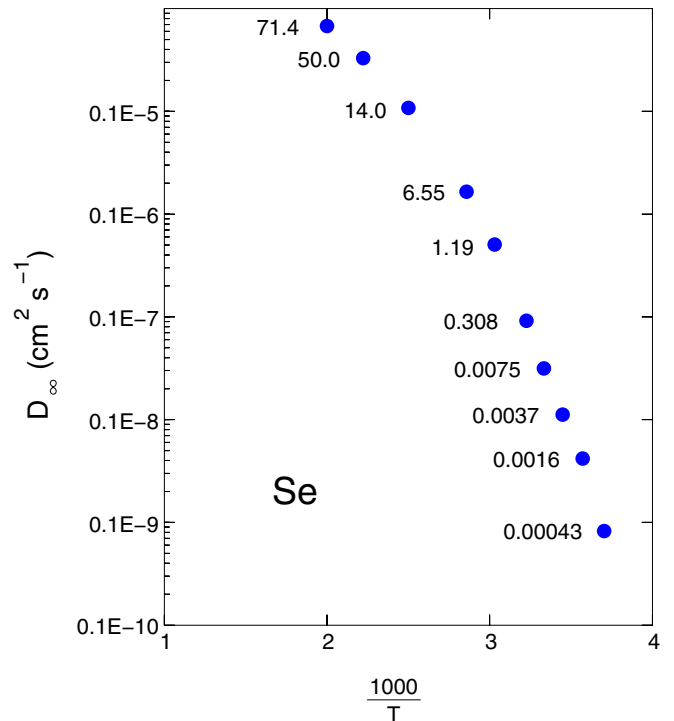


FIG. 7. Long-time diffusion coefficients $D_\infty(T)$ of Se between 500 K and 270 K and the corresponding values of $\alpha(T)$ [Eq. (6)] in units of ns⁻¹ [37] (FF simulations).

2. Power spectrum, vibrational DOS

The TwoPT program was used to calculate the vibrational and diffusive components of the power spectra, and the vibrational densities of states (vDOS; Fig. 8) are very similar to those calculated (from the melting point to below the glass transition temperature) by Caprion and Schober [55] for the FF used here. For 500 K, for example, there is a low-energy peak (2–5 meV), a shoulder near 14 meV, a pronounced minimum near 20 meV, and a second peak at 28–30 meV. All peaks move to lower frequencies (“soften”) as the temperature increases.

The calculated vDOS show pronounced similarities to the densities of states measured by inelastic neutron scattering for amorphous [83] and trigonal Se [84,85], and the trigonal form has also been studied theoretically. There are three atoms in the unit cell and nine phonon branches, and the identification of the acoustic branches with torsional vibrations, and the optical branches with bending (~ 13 meV) and stretching (~ 30 meV) nodes, has been carried over to the disordered phases as well. The low-frequency modes (~ 5 meV) have been attributed to interchain interactions (see [16] and references therein).

The small diffusive component of the DOS at all frequencies and temperatures is reflected in the fluidicity (Table I; see Sec. II B 2) and the temperature-dependent normalization of the vDOS. This differs strikingly from the situation in (metallic) liquid Sb [54] and liquid Bi [70], where diffusive components dominated at low frequencies. The diffusion coefficients D are given in Table I.

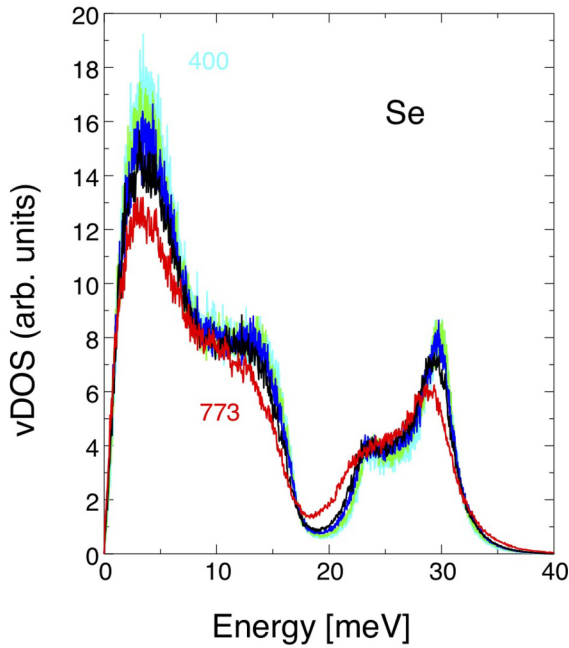


FIG. 8. Vibrational components of power spectra of Se from DF simulations at 400 K (cyan), 450 K (green), 500 K (blue), 600 K (black), and 773 K (red).

3. Dynamical structure factor

The dynamical structure factors $S(q, \omega)$ for selected q values were calculated from the DF trajectories at 400 K, 450 K, 500 K, 600 K, and 773 K using Eq. (9). Plots of the ratios to the static structure factors $S(q)$ are compared with experimental IXS results [52] in Figs. 9 (500 K) and 10 (773 K), respectively. Calculations for 400, 450, and 600 K are given in Figs. SF3, SF4, and SF5 of the Supplemental Material [75]. A Gaussian window function ($\sigma = 3$ meV) has been used to reduce numerical noise.

The overall agreement between the peak positions in theory and experiment is satisfactory for small q , but the calculated side peaks are more pronounced than in the experiment (523 K: below 0.5 ; 1023 K: below 0.4 \AA^{-1}). This effect is not due to discrepancies in the density assumed in the simulation. This value is closer to experiment at 523 K than at 773 K, but the agreement with experiment is better for small q values in the latter case (Fig. 10). Results for small q are naturally more sensitive to the simulation parameters (cell size, simulation time) than those for larger values of q , for which the peak positions and intensities agree well.

4. Current correlation functions, collective dynamics

Information about the collective dynamics can be obtained from the longitudinal and transverse current correlation functions (Sec. II B 4). The dispersion relations obtained from the peaks of $C_L(q, \omega)$ and $C_T(q, \omega)$ are shown in Fig. 11 for 500 K and 773 K. These results and those for 600 K are compared in Fig. SF6 of the Supplemental Material [75]. The linear relationship between ω and q below 0.7 \AA^{-1} for the LA modes indicates “phononlike” modes, and there is a minimum near $q = 1.8 \text{ \AA}^{-1}$, where there is a maximum in $S(q)$. A second,

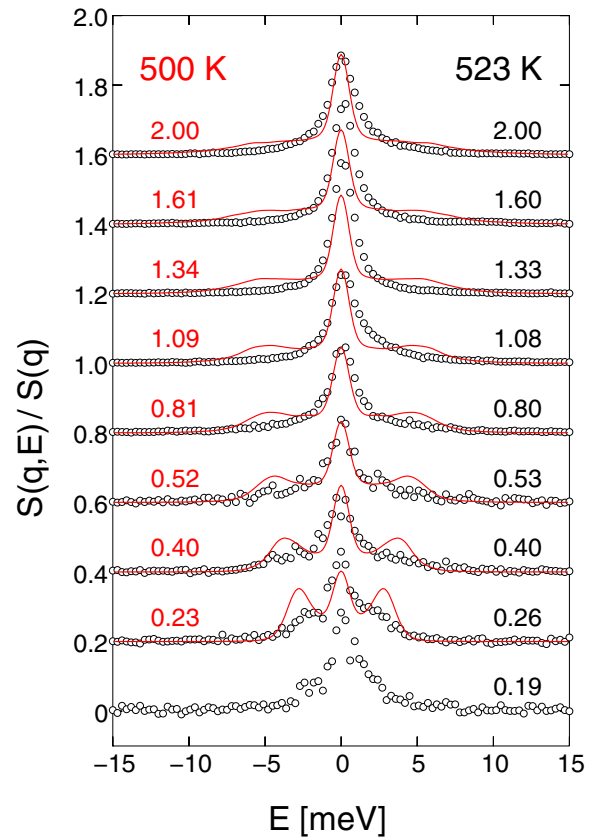


FIG. 9. Ratio of dynamical to static structure factors, $S(q, \omega)/S(q)$, for selected q values at 500 K. Red: DF with 3 meV Gaussian broadening; black, circles: experimental IXS at 523 K [52], with corresponding q values in \AA^{-1} .

weaker minimum occurs at approximately twice this wave vector. This does not imply that modes in this range of q are “phononlike,” but a process resembling umklapp scattering—sometimes viewed as a remnant “solidlike” feature—could occur in liquid Se. The overall agreement between the calculated dispersion curves and those derived from IXS data is satisfactory.

Sound velocities can be calculated from the linear part of the dispersion curves, and fits to the low q values in Fig. 11 give a longitudinal frequency-dependent phase velocity at 500 K of 1630 m/s, in good agreement with the IXS value of 1600 m/s and much larger than the adiabatic sound velocity measured at the melting point (1080 m/s, 494 K) [63]. “Positive dispersion” also occurs in glassy Se, where the extrapolated value of IXS measurements is 2000 m/s [86] and the longitudinal sound velocity at the glass temperature is 1780–1820 m/s [33]. It occurs in a wide range of liquids [87], although it is less pronounced (typically 10%–20%) in liquid metals [86]. The fit at 773 K yields a sound velocity of 1640 m/s compared with the IXS (1500 m/s) and adiabatic (880 m/s) values [63], so that positive dispersion is even more pronounced at higher temperatures. The measured sound velocities in the glassy [33] and crystalline [88] states are significantly higher than in the liquid [63], so that positive dispersion is sometimes viewed as a “solidlike” effect.

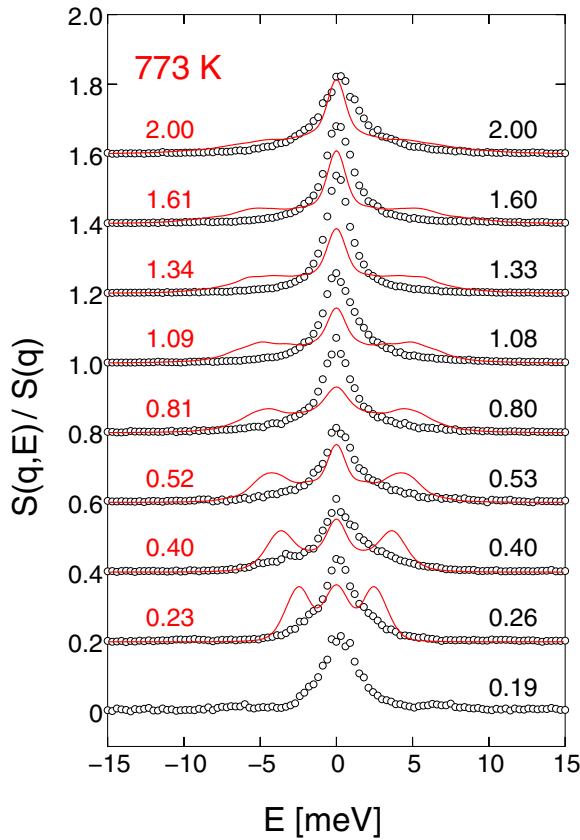


FIG. 10. Ratio of dynamical to static structure factors, $S(q, \omega)/S(q)$, for selected q values at 773 K. Red: DF with 3 meV Gaussian broadening; black, circles: experimental IXS at 773 K [52], with corresponding q values in \AA^{-1} .

Side peaks of the calculated $C_T(q, \omega)$ spectra are weaker than those on $C_L(q, \omega)$, but the transverse modes have been determined by fitting the quasielastic contribution at long wavelength to a Lorentzian function at $q = 0$ [69] and determining the peak position by fitting a single Gaussian function to the remainder. The dispersion of the transverse acoustic (TA) modes, also shown in Fig. 11, is linear at 500 K and 773 K, with transverse sound velocities of 760 m/s for 500 K, and 720 m/s for 773 K. The corresponding values are 870–900 m/s at the glass temperature [33] and 809 m/s in crystalline Se at 298 K [88].

5. Bond lifetimes

Bonds form and break at rates that depend on the temperature. In Fig. 12 we show the probability that a bond shorter than 2.8 \AA and present at time $t = 0$ is also present at time t . Table II provides further information concerning bonds that form and/or break during the simulations at 500 K and 773 K. The fixed bond cutoff may confuse “bond breaking” with bond stretching during vibration, and we show also in Fig. 12 the variation with time of the number of bonds (shorter than 2.4 \AA , but including those formed in the first 50 time steps) that are assumed to have “broken” when they are longer than 3.8 \AA . The temperature dependence is particularly striking. At 500 K, close to the melting point, all bonds so defined

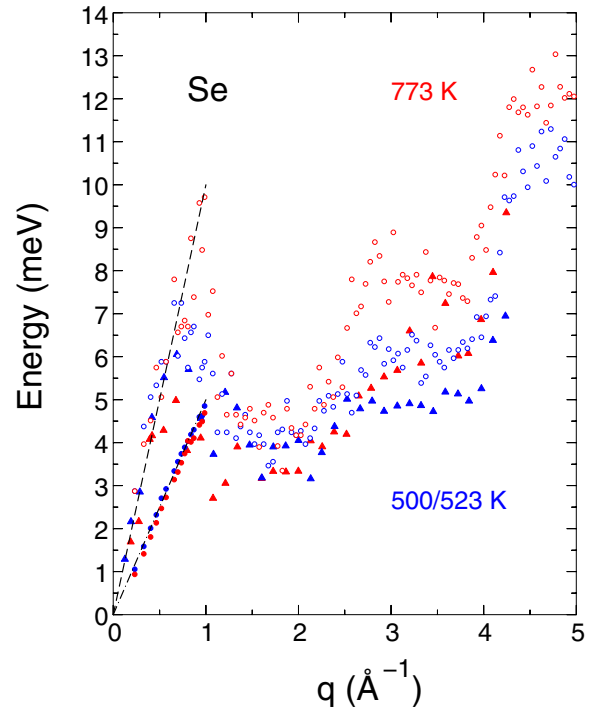


FIG. 11. Calculated longitudinal dispersion (open circles) at 500 K (blue) and 773 K (red) up to $q = 5.0 \text{ \AA}^{-1}$. Experimental results of Inui *et al.* for 523 K and 773 K are shown as blue and red triangles, respectively [52]. Full circles: Calculated frequencies of transverse modes; dashed and dot-dashed curves: sound velocities of 1500 m/s and 750 m/s, respectively.

remain throughout the simulation, while most bonds do not survive the simulation at 773 K. The FF simulations at 500 K (quench rate 10^{12} K/s) show that 38% of the bonds are still alive after 140 ps; 61% of the atoms have broken both bonds,

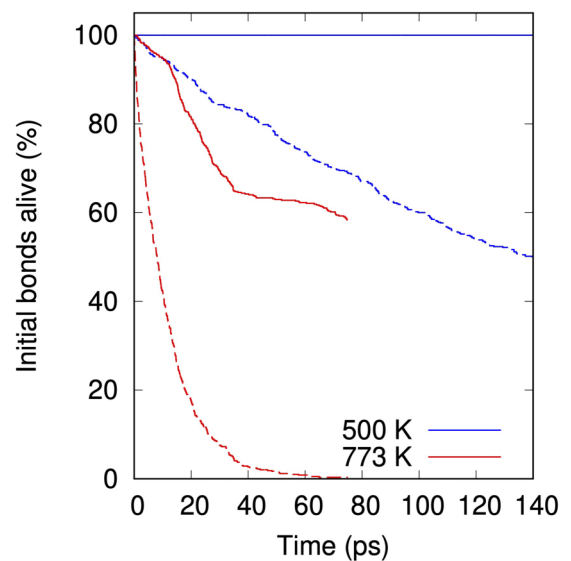


FIG. 12. Time dependence of number of active bonds in DF simulations at 500 K (blue) and 773 K (red). Dashed curves: Bonds break at 2.8 \AA ; full curves: bonds initially shorter than 2.4 \AA , break at 3.8 \AA .

TABLE II. Percentage of four categories of bonds in DF simulations at 500 K (140 ps) and 773 K (75 ps).

	500 K	773 K
Bond throughout	49.8	0.33
Initially present, broken at end	21.4	14.5
Formed during run, present at end	21.0	18.7
Formed and broken during run	7.8	66.4

35% have lost one bond, and just 4% have retained both. The simulation allows for bond reconnection. It is satisfying that the fraction of original bonds still alive after 140 ps is similar in the simulations at 500 K (DF: 50%; FF: 38%).

IV. DISCUSSION

The results of extensive molecular dynamics simulations of glassy and liquid Se using both density functional theory (DF; 600 atoms, 140 ps, 400–773 K) and a classical force field (FF; 5488 atoms, up to 800 ns, 290–500 K) have been analyzed to provide structural and dynamical information. The FF simulations indicate that the DF simulations below 500 K have not reached equilibrium. Comparison with experiment has been carried out where possible. The calculated structure factors $S(q)$ agree well with INS and IXS measurements at 523 K and 773 K [52], which encourages the use of DF/MD simulations in other disordered systems. A comparison of the the present (melt-quenched, MQ) results with DF/MD simulations of the as-deposited (AD) structure will be presented elsewhere [89].

The DF structures themselves are dominated by twofold-coordinated atoms, mainly chains, with a single chain occupying most of the cell at 500 K. There is a small ring component, a limited amount of branching at threefold-coordinated sites, and even fewer singly coordinated atoms at chain ends. There is more empty space and greater chain flexibility than found in similar simulations of Te [11,47]. Prescriptions for defining and determining the shape of cavities and their decomposition are not unique, but the Voronoi construction we use [65] leads to partial PDFs that suggest cavity ordering. This implies, of course, ordering in the Se atoms themselves.

The FF calculations at 350 K and 500 K show ring structures with up to 20 atoms, the most prominent being five-membered rings. DF calculations also give ring structures with five and more atoms, but the number of eight-membered

rings is vanishingly small, except at the highest simulation temperature 773 K. This is very surprising, since an equilibrium between Se_8 rings and chains has been postulated for more than 60 years as a possible structure for α -Se [16,18,20].

The focus on Se_8 rings has been based on the analogy to the group 16 neighbor S. Sulfur forms a liquid comprising S_8 and other homocyclic rings with up to 35 atoms [90] above the melting point (388 K) and below the onset of polymerization (432 K) to a mixture of rings and chains. Both S and Se form monoclinic structures comprising eight-membered rings with the “crown” (D_{4d}) structure, which are among the most stable of group 16 clusters [6,11]. Nevertheless, larger clusters, particularly S_{12} , have similar cohesive energies, and the number of chain isomers can greatly exceed the number of rings. In sulfur cluster anions, for example, they are favored over the more stable rings under certain experimental conditions [91]. The existence in liquid Se of Se_n rings with $n \neq 8$ is demonstrated by their presence in the neighboring vapor [24], so the sole focus on Se_8 rings is questionable.

Side peaks in the dynamical structure factor $S(q, \omega)$ indicate the presence of collective excitations, and the agreement with the dispersion found in IXS is satisfactory. $S(q, \omega)$ shows minima at q values where $S(q)$ has maxima (near $q = 1.8 \text{ \AA}^{-1}$ and $q = 3.6 \text{ \AA}^{-1}$). The low- q dispersion shows a sound velocity (1630 m/s, 500 K) that is close to the IXS experimental value, but much higher than the measured adiabatic sound velocity at the melting point (1080 m/s, 494 K) [63]. The pronounced “positive dispersion” in both experiment and theory at 773 K reflects the reduction of adiabatic sound velocities at higher temperatures. The spectra of the transverse current correlation functions $C_T(q, \omega)$ show inelastic peaks up to $q \sim 1 \text{ \AA}^{-1}$ with a linear dispersion corresponding to much lower sound velocities at low q (500 K: 760 m/s; 773 K: 720 m/s) than in the corresponding LA modes.

ACKNOWLEDGMENTS

We thank M. Inui for providing the original IXS data [52] and for encouragement, M. Ropo for contributions to the data analysis, and R. Steudel for helpful suggestions. We acknowledge gratefully the computer time provided by the JARA-HPC Vergabegremium (projects jiff05, jiff07) on the JARA-HPC partition of the supercomputers JUQUEEN and JURECA (Forschungszentrum Jülich) and at the CSC-IT Centre for Science (Espoo, Finland). We thank the Academy of Finland for financial support through its NANOIONICS program (Project No. 322832).

- [1] W. Hume-Rothery, The crystal structures of the elements of the B sub-groups and their connexion with the periodic table and atomic structures, *Philos. Mag.*, Ser. 7 **9**, 65 (1930).
- [2] L. Pauling, On the stability of the $\text{S}(8)$ molecule and the structure of fibrous sulfur, *Proc. Natl. Acad. Sci. USA* **35**, 495 (1949).
- [3] L. Pauling, *The Nature of the Chemical Bond and the Structure of Molecules and Crystals*, 3rd ed. (Cornell University Press, Ithaca, 1960), p. 135.

- [4] R. Steudel and B. Eckert, Solid sulfur allotropes, in *Elemental Sulfur and Sulfur-Rich Compounds I*, edited by R. Steudel (Springer, Berlin, 2003), pp. 1–80, and references therein.
- [5] D. Hohl, R. O. Jones, R. Car, and M. Parrinello, Structure of sulfur clusters using simulated annealing: S_2 to S_{13} , *J. Chem. Phys.* **89**, 6823 (1988).
- [6] R. O. Jones and P. Ballone, Density functional and Monte Carlo studies of sulfur. I. Structure and bonding in S_n rings and chains ($n = 2$ –18), *J. Chem. Phys.* **118**, 9257 (2003).

- [7] M. Springborg and R. O. Jones, Energy Surfaces of Polymeric Sulfur: Structure and Electronic Properties, *Phys. Rev. Lett.* **57**, 1145 (1986).
- [8] D. Hohl, R. O. Jones, R. Car, and M. Parrinello, The structure of selenium clusters Se_3 to Se_8 , *Chem. Phys. Lett.* **139**, 540 (1987).
- [9] M. Springborg and R. O. Jones, Sulfur and selenium helices: Structure and electronic properties, *J. Chem. Phys.* **88**, 2652 (1988).
- [10] R. O. Jones and D. Hohl, Structure, bonding, and dynamics in heterocyclic sulfur-selenium molecules, Se_xS_y , *J. Am. Chem. Soc.* **112**, 2590 (1990).
- [11] J. Akola and R. O. Jones, Structure and dynamics in amorphous tellurium and Te_n clusters: A density functional study, *Phys. Rev. B* **85**, 134103 (2012), and references therein.
- [12] Y. Tsuchiya, Localized two liquids phase and non-metal-metal transition in the liquid S-Te system, *J. Non-Cryst. Solids* **117-118**, 571 (1990).
- [13] M.-V. Coulet, R. Bellissent, and C. Bichara, Closed-loop miscibility gap in sulfur-tellurium melts: Structural evidence and thermodynamic modelling, *J. Phys.: Condens. Matter* **18**, 11471 (2006).
- [14] M. Hansen and K. Andenko, *Constitution of Binary Alloys*, 2nd ed. (McGraw-Hill, New York, 1958), pp. 1162, 1165-6, 1188-9.
- [15] G. Ghosh, R. C. Sharma, D. T. Li, and Y. A. Chang, The Se-Te (selenium-tellurium) system, *J. Phase Equilib.* **15**, 213 (1994).
- [16] S. N. Yannopoulos, Structure and photo-induced effects in elemental chalcogens: A review on Raman scattering, *J. Mater. Sci.: Mater. Electron.* **31**, 7565 (2020).
- [17] A. M. Kellas, The determination of the molecular complexity of liquid sulphur, *J. Chem. Soc., Trans.* **113**, 903 (1918).
- [18] A. V. Tobolsky and A. Eisenberg, Equilibrium polymerization of sulfur, *J. Am. Chem. Soc.* **81**, 780 (1959).
- [19] L. Henry, M. Mezouar, G. Garbarino, D. Sifré, G. Weck, and F. Datchi, Liquid-liquid transition and critical point in sulfur, *Nature (London)* **584**, 382 (2020).
- [20] A. Eisenberg and A. V. Tobolsky, Equilibrium polymerization of selenium, *J. Polym. Sci.* **46**, 19 (1960).
- [21] M. Misawa and K. Suzuki, Ring-chain transition in liquid selenium by a disordered chain model, *J. Phys. Soc. Jpn.* **44**, 1612 (1978).
- [22] R. Böhmer and C. A. Angell, Elastic and viscoelastic properties of amorphous selenium and identification of the phase transition between ring and chain structures, *Phys. Rev. B* **48**, 5857 (1993).
- [23] R. M. Martin, G. Lucovsky, and K. Hellawell, Intermolecular bonding and lattice dynamics of Se and Te, *Phys. Rev. B* **13**, 1383 (1976).
- [24] R. Steudel and E.-M. Strauss, *Homocyclic Selenium Molecules and Related Cations* (Academic Press, 1984), pp. 135-166.
- [25] K. Bernatz, I. Echeverría, S. Simon, and D. Plazek, Characterization of the molecular structure of amorphous selenium using recoverable creep compliance measurements, *J. Non-Cryst. Solids* **307-310**, 790 (2002).
- [26] W. W. Warren and R. Dupree, Structural and electronic transformations of liquid selenium at high temperature and pressure: A ^{77}Se NMR study, *Phys. Rev. B* **22**, 2257 (1980).
- [27] P. Jóvári, R. G. Delaplane, and L. Pusztai, Structural models of amorphous selenium, *Phys. Rev. B* **67**, 172201 (2003).
- [28] M. Marple, J. Badger, I. Hung, Z. Gan, K. Kovnir, and S. Sen, Structure of amorphous selenium by 2D ^{77}Se NMR spectroscopy: An end to the dilemma of chain versus ring, *Angew. Chem.* **129**, 9909 (2017).
- [29] W. Zhu, B. G. Aitken, and S. Sen, Communication: Observation of ultra-slow relaxation in supercooled selenium and related glass-forming liquids, *J. Chem. Phys.* **148**, 111101 (2018).
- [30] M. Inui, Y. Kajihara, K. Kimura, K. Matsuda, K. Ohara, S. Tsutsui, D. Ishikawa, and A. Q. Baron, Inelastic x-ray scattering studies on dynamic structure factor of polymeric liquid Se under pressure, in *Proceedings for the XV Liquid and Amorphous Metals (LAM-15) International Conference*, edited by L. Wang and H. Liu, AIP Conf. Proc. No. 1673 (AIP, New York, 2015), p. 020002, and references therein.
- [31] K. Tamura, Structural changes and the metal-non-metal transition in supercritical fluids, *J. Non-Cryst. Solids* **205-207**, 239 (1996).
- [32] K. Maruyama, S. Hiroi (Sato), H. Endo, H. Hoshino, T. Odagaki, and F. Hensel, The packing of helical and zigzag chains and distribution of interstitial voids in expanded liquid Se near the semiconductor to metal transition, *EPJ Web Conf.* **151**, 01003 (2017).
- [33] V. Kozhevnikov, W. Payne, J. Olson, A. Allen, and P. Taylor, Sound velocity in liquid and glassy selenium, *J. Non-Cryst. Solids* **353**, 3254 (2007).
- [34] Y. Tsuchiya, Thermodynamic evidence for a structural transition of liquid Te in the supercooled region, *J. Phys.: Condens. Matter* **3**, 3163 (1991).
- [35] R. O. Jones, Density functional theory: Its origins, rise to prominence, and future, *Rev. Mod. Phys.* **87**, 897 (2015).
- [36] N. G. Almaraz, E. Enciso, and F. J. Bermejo, Structure and dynamics of selenium chain melts: A molecular dynamics study, *J. Chem. Phys.* **99**, 6876 (1993).
- [37] D. Caprion and H. R. Schober, Structure and relaxation in liquid and amorphous selenium, *Phys. Rev. B* **62**, 3709 (2000).
- [38] A. H. Goldan, C. Li, S. J. Pencycook, J. Schneider, A. Blom, and W. Zhao, Molecular structure of vapor-deposited amorphous selenium, *J. Appl. Phys.* **120**, 135101 (2016).
- [39] H. R. Schober, Diffusion, relaxation, and aging of liquid and amorphous selenium (unpublished).
- [40] P. Ballone and R. O. Jones, Density functional and Monte Carlo studies of sulfur. II. Equilibrium polymerization of the liquid phase, *J. Chem. Phys.* **119**, 8704 (2003).
- [41] C. Bichara, A. Pellegatti, and J.-P. Gaspard, Chain structure of liquid selenium investigated by a tight-binding Monte Carlo simulation, *Phys. Rev. B* **49**, 6581 (1994).
- [42] C. Oligschleger, R. O. Jones, S. M. Reimann, and H. R. Schober, Model interatomic potential for simulations in selenium, *Phys. Rev. B* **53**, 6165 (1996) (parameter a in Table I should be 9281.2, $\alpha = -7.9284$).
- [43] D. Hohl and R. O. Jones, First principles MD simulation of liquid and amorphous selenium, *J. Non-Cryst. Solids* **117-118**, 922 (1990); First-principles molecular-dynamics simulation of liquid and amorphous selenium, *Phys. Rev. B* **43**, 3856 (1991).
- [44] F. Shimojo, K. Hoshino, M. Watabe, and Y. Zempo, The semiconductor-metal transition in fluid selenium: An *ab initio* molecular-dynamics simulation, *J. Phys.: Condens. Matter* **10**, 1199 (1998).

- [45] F. Kirchhoff, G. Kresse, and M. J. Gillan, Structure and dynamics of liquid selenium, *Phys. Rev. B* **57**, 10482 (1998).
- [46] R. Stadler and M. J. Gillan, First-principles molecular dynamics studies of liquid tellurium, *J. Phys.: Condens. Matter* **12**, 6053 (2000).
- [47] J. Akola, R. O. Jones, S. Kohara, T. Usuki, and E. Bychkov, Density variations in liquid tellurium: Roles of rings, chains, and cavities, *Phys. Rev. B* **81**, 094202 (2010).
- [48] P. Košťál and J. Málek, Viscosity of selenium melt, *J. Non-Cryst. Solids* **356**, 2803 (2010), and references therein.
- [49] A. Axmann, W. Gissler, A. Kollmar, and T. Springer, The investigation of atomic motions in crystalline, amorphous and liquid selenium, and in crystalline and liquid tellurium by neutron spectroscopy, *Discuss. Faraday Soc.* **50**, 74 (1970).
- [50] A. Chiba, Y. Ohmasa, M. Yao, O. Petrenko, and Y. Kawakita, Quasielastic neutron scattering of liquid $\text{Te}_{50}\text{Se}_{50}$ in the semiconductor-to-metal transition range, *J. Phys. Soc. Jpn.* **71**, 504 (2002); A. Chiba, Y. Ohmasa, and M. Yao, Vibrational, single-particle-like, and diffusive dynamics in liquid Se, Te, and $\text{Te}_{50}\text{Se}_{50}$, *J. Chem. Phys.* **119**, 9047 (2003).
- [51] K. Maruyama, H. Endo, and H. Hoshino, Short- and intermediate-range structures of liquid Rb-Se mixtures, *J. Phys. Soc. Jpn.* **74**, 3213 (2005).
- [52] M. Inui, S. Hosokawa, K. Matsuda, S. Tsutsui, and A. Q. R. Baron, Collective dynamics and de Gennes narrowing in polymeric liquid Se: High-resolution inelastic x-ray scattering, *Phys. Rev. B* **77**, 224201 (2008); M. Inui (private communication).
- [53] M. Ropo, J. Akola, and R. O. Jones, Collective excitations and viscosity in liquid Bi, *J. Chem. Phys.* **145**, 184502 (2016).
- [54] R. O. Jones, O. Ahlstedt, J. Akola, and M. Ropo, Density functional study of structure and dynamics in liquid antimony and Sb_n clusters, *J. Chem. Phys.* **146**, 194502 (2017).
- [55] D. Caprion and H. R. Schober, Vibrational density of states of selenium through the glass transition, *J. Chem. Phys.* **114**, 3236 (2001).
- [56] D. Caprion and H. R. Schober, Influence of the quench rate and the pressure on the glass transition temperature in selenium, *J. Chem. Phys.* **117**, 2814 (2002).
- [57] M. Parrinello and A. Rahman, Polymorphic transitions in single crystals: A new molecular dynamics method, *J. Appl. Phys.* **52**, 7182 (1981).
- [58] L. Verlet, Computer “experiments” on classical fluids. I. Thermodynamical properties of Lennard-Jones molecules, *Phys. Rev.* **159**, 98 (1967).
- [59] CPMD V3.15 © IBM Corp. 1990–2013, © MPI für Festkörperforschung Stuttgart 1997–2001.
- [60] N. Troullier and J. L. Martins, Efficient pseudopotentials for plane-wave calculations, *Phys. Rev. B* **43**, 1993 (1991).
- [61] J. P. Perdew, A. Ruzsinszky, G. I. Csonka, O. A. Vydrov, G. E. Scuseria, L. A. Constantin, X. Zhou, and K. Burke, Restoring the Density-Gradient Expansion for Exchange in Solids and Surfaces, *Phys. Rev. Lett.* **100**, 136406 (2008).
- [62] C. L. Yaws, Liquid density of the elements, *Chem. Eng. –New York* **114**, 44 (2007).
- [63] Y. Tsuchiya, R. Satoh, and F. Kakinuma, The velocity of sound in the liquid S-Se alloy, *J. Non-Cryst. Solids* **250-252**, 468 (1999).
- [64] S. Nosé, A unified formulation of the constant temperature molecular dynamics methods, *J. Chem. Phys.* **81**, 511 (1984); W. G. Hoover, Canonical dynamics: Equilibrium phase-space distributions, *Phys. Rev. A* **31**, 1695 (1985).
- [65] I. Heimbach, F. Rhiem, F. Beule, D. Knodt, J. Heinen, and R. O. Jones, pyMolDyn: Identification, structure, and properties of cavities/vacancies in condensed matter and molecules, *J. Comput. Chem.* **38**, 389 (2017).
- [66] W. Klyne and V. Prelog, Description of steric relationships across single bonds, *Experientia* **16**, 521 (1960).
- [67] S.-T. Lin, M. Blanco, and W. A. Goddard, The two-phase model for calculating thermodynamic properties of liquids from molecular dynamics: Validation for the phase diagram of Lennard-Jones fluids, *J. Chem. Phys.* **119**, 11792 (2003); T. A. Pascal, S.-T. Lin, and W. A. Goddard III, Thermodynamics of liquids: Standard molar entropies and heat capacities of common solvents from 2PT molecular dynamics, *Phys. Chem. Chem. Phys.* **13**, 169 (2011).
- [68] H. R. Schober, Diffusion in a model metallic glass: Heterogeneity and ageing, *Phys. Chem. Chem. Phys.* **6**, 3654 (2004).
- [69] J.-P. Hansen and I. R. McDonald, *Theory of Simple Liquids*, 4th ed. (Academic Press, Oxford, 2013).
- [70] J. Akola, N. Atodiresei, J. Kalikka, J. Larrucea, and R. O. Jones, Structure and dynamics in liquid bismuth and Bi_n clusters: A density functional study, *J. Chem. Phys.* **141**, 194503 (2014).
- [71] A. Einstein, Über die von der molekularkinetischen Theorie der Wärme geforderte Bewegung von in ruhenden Flüssigkeiten suspendierten Teilchen, *Ann. Phys. (Leipzig)* **322**, 549 (1905).
- [72] S. Hamada, N. Yoshida, and T. Shirai, On the viscosity of liquid selenium, *Bull. Chem. Soc. Jpn.* **42**, 1025 (1969).
- [73] A. Eisenberg and L. A. Teter, Relaxation mechanisms in polymeric sulfur, *J. Phys. Chem.* **71**, 2332 (1967).
- [74] W. Zhu, I. Hung, Z. Gan, B. Aitken, and S. Sen, Dynamical processes related to viscous flow in a supercooled arsenic selenide glass-forming liquid: Results from high-temperature ^{77}Se NMR spectroscopy, *J. Non-Cryst. Solids* **526**, 119698 (2019).
- [75] See Supplemental Material at <http://link.aps.org/supplemental/10.1103/PhysRevB.102.104202> provides plots of PDF $g(r)$ and structure factor $S(q)$, calculated (DF/MD) dynamical structure factors $S(q, \omega)/S(q)$ for selected values of ω at 400, 450, and 600 K, and calculated dispersion of longitudinal and transverse modes at 500, 600, and 773 K. Partial PDF for Se-cavity and cavity-cavity are given for 500 K and 773 K, as are coordinate files for the final structures of the simulations at 500 K, 600 K, and 773 K.
- [76] See, for example, <http://jmol.sourceforge.net>.
- [77] R. Steudel, Hypervalent defects in amorphous selenium and similar lone-pair semiconductors, *J. Non-Cryst. Solids* **83**, 63 (1986), and references therein.
- [78] A. V. Kolobov, H. Oyanagi, K. Tanaka, and K. Tanaka, Structural study of amorphous selenium by *in situ* EXAFS: Observation of photoinduced bond alternation, *Phys. Rev. B* **55**, 726 (1997).
- [79] K. Maruyama, S. Tamaki, S. Takeda, and M. Inui, Reverse Monte Carlo simulations in liquid chalcogens, *J. Phys. Soc. Jpn.* **62**, 4287 (1993).
- [80] L. Červinka, Medium-range ordering in non-crystalline solids, *J. Non-Cryst. Solids* **90**, 371 (1987).
- [81] S. R. Elliott, The origin of the first sharp diffraction peak in the structure factor of covalent glasses and liquids, *J. Phys.: Condens. Matter* **4**, 7661 (1992).

- [82] W. A. Phillips, U. Buchenau, N. Nücker, A.-J. Dianoux, and W. Petry, Dynamics of Glassy and Liquid Selenium, *Phys. Rev. Lett.* **63**, 2381 (1989).
- [83] F. Gompf, The phonon densities of states of trigonal, vitreous and red amorphous selenium, *J. Phys. Chem. Solids* **42**, 539 (1981).
- [84] W. D. Teuchert, R. Geick, G. Landwehr, H. Wendel, and W. Weber, Lattice dynamics of trigonal selenium. I. Phonon spectra, *J. Phys. C: Solid State Phys.* **8**, 3725 (1975).
- [85] L. M. Needham, M. Cutroni, A. J. Dianoux, and H. M. Rosenberg, A study of the vibrational spectrum of amorphous and crystalline SeTe samples by inelastic neutron scattering, *J. Phys.: Condens. Matter* **5**, 637 (1993).
- [86] T. Scopigno, R. Di Leonardo, G. Ruocco, A. Q. R. Baron, S. Tsutsui, F. Bossard, and S. N. Yannopoulos, High Frequency Dynamics in a Monatomic Glass, *Phys. Rev. Lett.* **92**, 025503 (2004).
- [87] T. Scopigno, G. Ruocco, and F. Sette, Microscopic dynamics in liquid metals: The experimental point of view, *Rev. Mod. Phys.* **77**, 881 (2005).
- [88] D. Royer and E. Dieulesaint, Elastic and piezoelectric constants of trigonal selenium and tellurium crystals, *J. Appl. Phys.* **50**, 4042 (1979).
- [89] J. Kalikka, J. Akola, and R. O. Jones (unpublished).
- [90] R. Steudel, Liquid sulfur, in *Elemental Sulfur and Sulfur-Rich Compounds I*, edited by R. Steudel (Springer, Berlin, 2003), pp. 81–116.
- [91] S. Hunsicker, R. O. Jones, and G. Ganteför, Rings and chains in sulfur cluster anions S^- to S_7^- : Theory (simulated annealing) and experiment (photoelectron detachment), *J. Chem. Phys.* **102**, 5917 (1995).